Journal of
Marine Science and Engineering

MDPI

Article

Dynamic Interactions of a Cable-Laying Vessel with a Submarine Cable during Its Landing Process

Jianxun Kuang [1], Guodong Chen [1], Zhoulong Yuan [1], Xiajun Qi [1], Qianhao Yu [1] and Zhen Liu [2,*]

1 Zhejiang Qiming Electric Power Engineering Co., Ltd., Zhoushan 316000, China; zsxm2017@126.com (J.K.); chenguodong662702@126.com (G.C.); 13868209580@163.com (Z.Y.); xiajun_7@163.com (X.Q.); yuqianhao665219@126.com (Q.Y.)
2 Department of Ocean Engineering, College of Engineering, Ocean University of China, Qingdao 266100, China
* Correspondence: liuzhen@ouc.edu.cn

Abstract: The rapid development of offshore electricity grid construction has led to a great demand for submarine cable deployment. In this study, a numerical model is established based on the commercial software ANSYS-AQWA to investigate the dynamic interactions between a cable-laying vessel and a submarine cable during its landing process, which has not yet been reported and is critical to the safety of the cable. The numerical model was validated by an experimental test on the mooring stability of a vessel conducted in a wave tank. The effects of the cable length, the current velocity, the incident wave, and the wind direction on vessel stability and the tensions in the mooring lines and cable were investigated. When the cable length is short, the submarine cable acts as a mooring cable that can stabilize the hull, but it is not safe to apply force to the submarine cable. At the same time, an increase in the current speed also increases the tensile force of the submarine cable. The influence of different incident wave directions and wind directions on the stability and tension of ships in mooring lines and cables was studied, and the most unfavorable environmental conditions for submarine cable laying were determined under different environmental conditions.

Keywords: cable-laying vessel; submarine cable; dynamic interactions; numerical simulation

check for updates

Citation: Kuang, J.; Chen, G.; Yuan, Z.; Qi, X.; Yu, Q.; Liu, Z. Dynamic Interactions of a Cable-Laying Vessel with a Submarine Cable during Its Landing Process. *J. Mar. Sci. Eng.* **2022**, *10*, 774. https://doi.org/10.3390/jmse10060774

Academic Editor: Spyros A. Mavrakos

Received: 27 April 2022
Accepted: 31 May 2022
Published: 3 June 2022

1. Introduction

The rapid development of offshore resources, including islands, underwater minerals, wind and marine energies, and aquatic products, necessitates more human activities that involve electricity supply and transmission. Electricity is mainly transmitted by submarine cables in offshore circumstances. The offshore power grid is the same as the onshore grid, which needs more submarine cables to be laid to interconnect the networks [1,2]. Consequently, laying submarine cables safely has become an important mission for offshore electricity transmission engineering.

Landing cables is the most difficult part of the entire process of cable laying. In addition, a critical issue to prevent cable damage is to control the tension in the cable during laying [3,4]. Compared to the traditional landing methodology, floaters could be employed to provide additional buoyancy to the floating cable and prevent possible overloaded friction and bending stress concentration [5]. On the other hand, a reasonable design and deployment of the mooring lines could enhance the stability of a cable-laying vessel in complicated sea states and reduce the tension in the cable from the vessel motion. Therefore, the dynamic interactions between the cable and floaters, vessel, and mooring lines play a critical role in the safety and reliability of cable-laying engineering.

For the stability of the ships and offshore platforms, due to the large structures and multiple external and internal loads, numerical simulations have become a popular methodology to study the effects of environmental forces and structural parameters on the motion of ships and platforms. Hu et al. investigated the kinematic response of a liquified natural gas ship under the joint effects of waves, streams, and winds [6]. Shigunov et al. reported the dynamic stability of an offshore service vessel under various operating conditions [7]. Liu et al. preliminarily estimated the intensity response of a deep-water ship in still water and under regular wave conditions [8]. Putra et al. evaluated the tilting stability of a flat shell ship under different environmental conditions [9]. Roy et al. conducted an integrated numerical analysis on the motion and structural responses of an offshore spar platform to irregular waves [10]. Banik et al. investigated the effects of incident wave direction on the dynamic responses of a spar offshore platform [11]. Wang et al. proposed a motion equation and used it to study the influences of wave group parameters on the ship motions in random wave groups [12]. Su et al. investigated the seakeeping performance of a variable-structure ship under regular and irregular waves [13].

The mooring line is also important for the stability of the ships. Liu conducted a dynamic analysis of mooring lines and investigated their damping effects on floating platforms [14]. Sarkar et al. proposed a dynamic stiffness method to handle the kinematic problems of mooring lines [15] and considered seabed friction in a linear analysis under irregular wave conditions [16]. Gao et al. studied the mooring performance of a multi-body floating system under the joint impact of the wind, waves, and waterflow [17]. Nie et al. refined the mooring forces using a time-domain method under environmental forces [18]. Zheng et al. investigated the tensions of the bow–stern mooring system of a single ship under the combination impact of external loads [19]. Pham proposed a computational fluid dynamic model to simulate the tensions of mooring lines under various operating conditions [20]. Based on the experimental and numerical results, Nguyen et al. proposed an empirical formula to calculate the tension of mooring lines for oil ships and studied the effects of waterflow on mooring line tension [21].

For the stability and dynamic positioning of a cable-laying vessel, Fu et al. proposed a self-adapted surface tracking control method [22]. Yang et al. analyzed the dynamic responses of a submarine cable during the motion of a laying vessel and the kinematic characteristics of a cable during its laying [23,24]. Under extremely shallow water conditions, Cavefors et al. studied the motion effects of a cable-laying vessel on the tensions of the mooring lines under various wave conditions [25]. Zhang et al. and Wang et al. analyzed the effects of the vessel velocity, water depth, and length of the cable using models that coupled the vessel with the submarine cable [26,27]. In addition, related scholars carried out research related to cable structure health monitoring [28,29]. Drissi-Habti M et al. simulated the real strain of copper wire in high-voltage electric transport phases using an optical fiber sensor (FOS) [30].

From the literature review, it can be seen that most previous studies individually focused on the vessel stability and tensions of submarine cables, while the dynamic interactions between the moored cable-laying vessel and submarine cables during the cable landing process have not yet been reported. In this study, due to the engineering demands of the Qifan No. 9 vessel, a numerical model was established based on the commercial computational fluid dynamic software Ansys-AQWA and validated by the corresponding experimental data. The effects of the submarine cable length, current velocity, incident wave, and wind direction on vessel stability and tensions in the mooring lines and cables were investigated.

2. Numerical Model

2.1. Governing Equations

In this study, air and water are idealized and assumed to be incompressible, irrotational, and non-viscous. Based on the three-dimensional potential flow theory, the velocity potential ϕ satisfies the Laplace equation in the flow field [31]:

$$\nabla^2\phi = 0 \tag{1}$$

Introducing the complex form of the velocity potential ϕ:

$$\phi = Re\left(\varphi e^{-i\,\omega t}\right) \tag{2}$$

where ω is the frequency of incident waves and t is the time.

The velocity potential can be divided into three parts: the incident potential ϕ_I, the diffraction potential ϕ_D, and the radiation potential ϕ_R, which all satisfy the Laplace equation. In addition, the incident potential can be written as follows:

$$\phi_I = \frac{A_i g}{\omega}\frac{\cos hk_i(z+d)}{\cosh kd}e^{[ik(x\cos\beta + y\sin\beta)]} \tag{3}$$

where A_i is the incident wave amplitude, k_i is the wave number, h is the water depth, g is the gravitational acceleration, and β is the intersection angle between the incident wave direction and the positive direction of the x-axis.

The governing equation of the diffraction potential; boundary conditions for the free surface, seabed, and rigid body surface; and definite condition at infinity can be written as follows:

$$\nabla^2\varphi_D = 0 \tag{4}$$

$$\frac{\partial\varphi_D}{\partial z} - \frac{\omega^2}{g}\varphi_D = 0\ (z=0) \tag{5}$$

$$\frac{\partial\varphi_D}{\partial z} = 0\ (z=-d) \tag{6}$$

$$\frac{\partial\varphi_D}{\partial n} = -\frac{\partial\varphi_I}{\partial n} \tag{7}$$

$$\lim_{R\to\infty}\sqrt{R}\left(\frac{\partial\varphi_D}{\partial R} - iK\varphi_D\right) = 0 \tag{8}$$

If six degrees of freedom (DOFs) are considered, the radiation potential can be expressed as follows:

$$\varphi_R = i\omega\sum_{j=1}^{6}\varepsilon_j\varphi_j \tag{9}$$

The governing equation of the radiation potential; the boundary conditions for the free surface, seabed, and rigid body surface; and definite condition at infinity can be written as follows:

$$\nabla^2\varphi_R = 0 \tag{10}$$

$$\frac{\partial\varphi_R}{\partial z} - \frac{\omega^2}{g}\varphi_R = 0\ (z=0) \tag{11}$$

$$\frac{\partial\varphi_R}{\partial z} = 0\ (z=-d) \tag{12}$$

$$\frac{\partial\varphi_j}{\partial n} = i\omega n_j (j = 1,\ 2,\ \ldots,\ 6) \tag{13}$$

$$\lim_{R\to\infty}\sqrt{R}\left(\frac{\partial\phi_R}{\partial R} - ik\phi_R\right) = 0 \tag{14}$$

where ε_j represents the motion at the jth degree of freedom, and φ_j represents the radiation potential caused by the motion at the jth degree of freedom. n is the unit vector, which is perpendicular to the floater boundary and points to the floater.

As the velocity potential and the surface pressure are determined, the wave force acting on the body can be calculated as follows:

$$(m_{ij} + \mu_{ij})\ddot{x}_j + \lambda_{ij}x_j + k_{ij}x = f_i (i = 1, 2\ldots 6) \tag{15}$$

where m is the quality matrix, μ is the added mass matrix, λ is the damping coefficient matrix, and k is the restoring force matrix. f_i is the first-order wave force acting on the body.

Following the API codes [32], the wind force F_w and the water current force F_{cs} are estimated as follows:

$$F_w = C_w \sum (C_s C_h A) V_w{}^2 \tag{16}$$

$$F_{cs} = C_{ss} C_d A V_c^2 \tag{17}$$

where C_w is the wind force coefficient, which is commonly defined as 0.615 $\mathrm{Ns^2/m^4}$. C_s and C_h are the ship shape coefficient and ship height coefficient, respectively. A is the projected area of the ship in the direction perpendicular to the incident wind direction, and V_w is the wind velocity. C_{ss} is the water current force coefficient, which is commonly defined as 515.62 $\mathrm{Ns^2/m^4}$. C_d is the drag coefficient of the water flow, which is 0.5 for a cylinder and 1.5 for a flat plate. A is the projected area of the ship in the direction perpendicular to the incident water current, and V_c is the water current velocity.

2.2. Numerical Model Setup

The ship model is established based on the cable-laying vessel Qifan No. 9, designed and owned by Zhejiang Qiming Electric Power Group Co. Ltd. (Zhoushan, China). As shown in Figure 1, it is the first 5000 t professional vessel for submarine cable engineering [33]. The vessel is equipped with an advanced cable tray and a clean room for cable connection on site. The single construction distance for 220 kV voltage level cables can be enhanced from 30.0 km to 60.0 km. The eight-point mooring system enables the vessel to resist force 10 winds.

Figure 1. Qifan No. 9 cable-laying vessel.

The governing equations are solved in the commercial software Ansys-AQWA. The cable-laying vessel is modeled in Design Modeler integrated in Workbench, as shown in Figure 2. As the model structure affects the complexity and quality of the generated grids, and subsequently the computational time and accuracy, the vessel structure is simplified, and the extraction is conducted. The vessel draught is preset with centers of mass and gravity. As the positions of anchor points and fairleads on the vessel are fixed, the material and properties of the mooring lines are set in the model. The floating submarine cable for the landing process is also set in the related modules following the same procedure, as shown in Figure 2a. According to the vessel shape and size, the greatest length of the grid is 1.5 m. The primary grid shape is quadrangular with a total number of 11,371, as shown in Figure 2b.

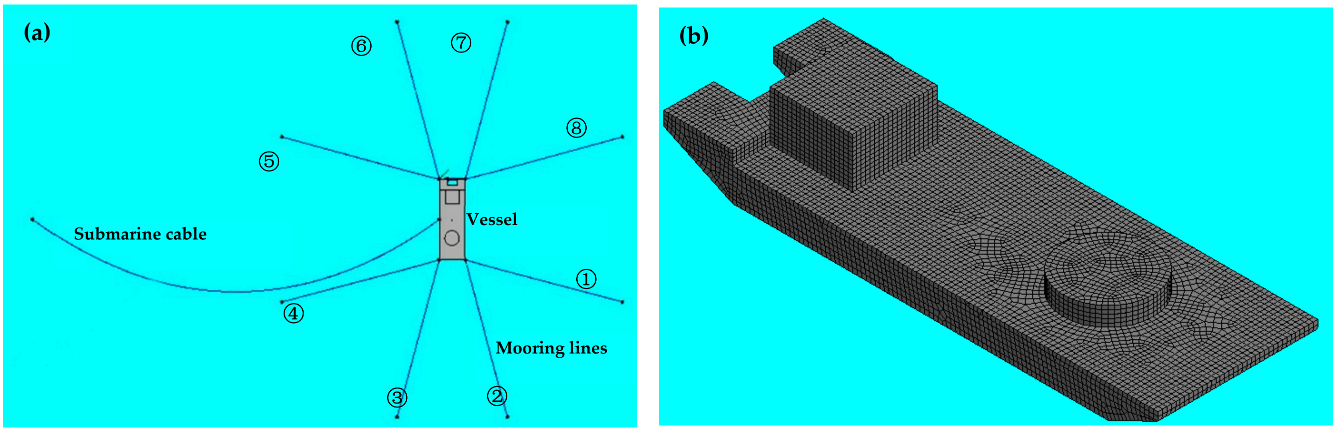

Figure 2. Numerical model for the moored vessel and landing submarine cable. (**a**) Model setup for the vessel, mooring lines ①–⑧, and submarine cable. (**b**) Mesh structures of the vessel.

The simulation modules in the software Ansys-AQWA can be accessed from the Hydrodynamic Responses and Hydrodynamic Diffraction modules in the Analysis Systems in Workbench. The module AQWA-LINE is responsible for the diffraction and radiation calculations, and AQWA-DRIFT is employed for the time-domain analysis of the second-order Morison forces in irregular waves. The AQWA-FER module can be used for the frequency-domain analysis with irregular waves. The nonlinear time-domain simulation of regular and irregular waves can be calculated for the survival conditions in the AQWA-NAUT. The module AQWA-Cable Dynamics can be integrated for simulations where the cables or mooring lines should be considered.

The cable-laying missions conducted by Qifan No. 9 shall employ the floaters to provide additional buoyancy to the landing cables in the future, as shown in Figure 3. Considering the primary function of the floaters, they are simplified as the uniform distributed buoyancy acting on the cable. During the time-domain calculations, the computational time step is 0.5 s with a total computation period of over 20,000 s.

Figure 3. Floaters for submarine cable landing. Adapted from [34].

3. Experimental Validation of the Numerical Model

3.1. Experiment Setup

An experimental test was conducted to validate the numerical model. The experiments were performed in the wave tank of the Shandong Provincial Key Laboratory of Ocean Engineering, Ocean University of China. Considering the vessel size, the tank size and capability, and the environmental conditions, a model scale ratio of 1:49 was used following the Froude similarity law. The model vessel was designed with the parameters listed in Table 1 and manufactured using wood, as shown in Figure 4a. In addition, the ballast of the vessel was carefully adjusted to satisfy the model weight, draught, and displacement. The truncation method was employed for the modeled mooring lines to adapt to the shallow testing water depth in the tank.

Table 1. Parameters for the prototype and model vessels.

Parameters	Prototype Vessel	Model Vessel
Vessel length (m)	99.0	2.02
Molded breadth (m)	32.0	0.65
Molded depth (m)	6.5	0.134
Maximum draft (m)	4.8	0.098
Maximum displacement (t)	14,300	0.122 *
Diameter of mooring lines (mm)	50.0	1.02

* Model weight: 0.069 t; ballast weight: 0.053 t.

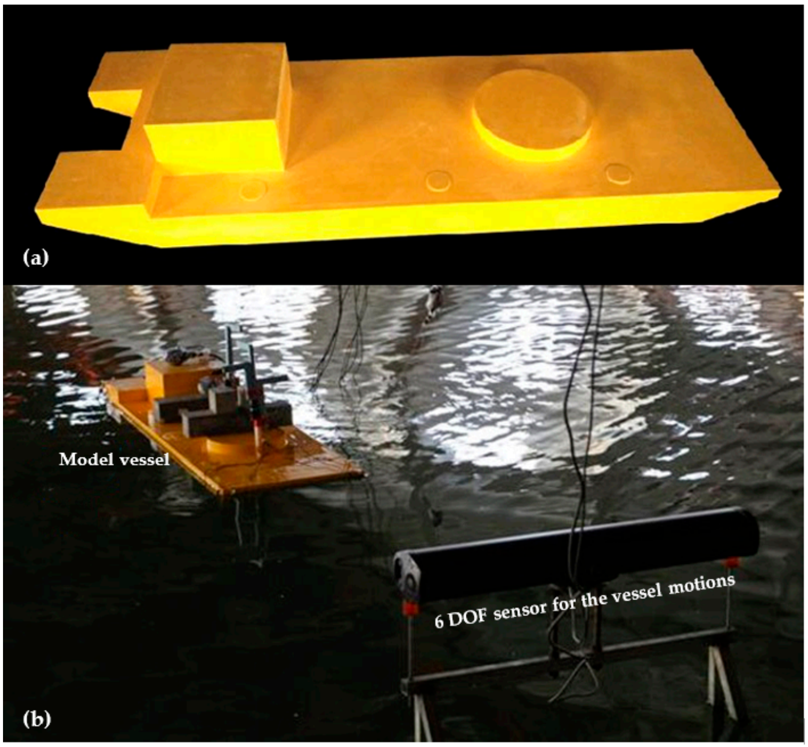

Figure 4. (**a**) Model vessel. (**b**) Experimental setup for validation.

The model vessel was moored following the same distribution pattern shown in Figure 2a. Only typical regular and irregular waves were used as the primary environmental conditions. The incident wave direction was perpendicular to the bow-to-stern of the vessel. The motions of the vessel in six DOFs were measured using an optical motion sensor, as shown in Figure 4b. The tensions in the mooring lines were recorded by the force transducers installed between the mooring lines and the vessel. The regular wave condition included a wave height of H = 0.05 m and a wave period of T = 1.5 s. Furthermore, the irregular wave condition included a significant wave height of H_S = 0.05 m and a significant wave period of T_S = 1.5 s. The JONSWAP spectrum was used to generate the irregular wave scenario with an enhanced peak factor of γ = 3.3.

The kinematic responses in six DOFs and tensions in the mooring lines and submarine cable are nondimensionalized. The nondimensional translational and rotational motions in six DOFs $\overline{\zeta}_i$ and $\overline{\zeta}_j$ can be expressed as follows [35]:

$$\overline{\zeta}_i = \frac{\zeta_i}{H_0}(i = 1,\ 2,\ 3), \overline{\zeta}_j = \frac{\zeta_j}{kH_0}\ (j = 4,\ 5,\ 6) \tag{18}$$

where k and H_0 represent the wave number and incident wave height, respectively. ζ_i and ζ_j are the corresponding dimensional motions. $i = 1, 2, 3$, ζ_i represent the heaving, swaying, and surging motions, respectively. $j = 4, 5, 6$, ζ_j represent the rolling, pitching, and yawing motions, respectively.

The nondimensional tension $\overline{F}$ can be expressed as follows:

$$\overline{F} = \frac{F}{T_M} \tag{19}$$

where F is the tension in the mooring lines or the submarine cable. T_M is the designed breaking loads for the mooring line and submarine cable with values of 950 kN and 190 kN, respectively.

3.2. Validation of Numerical Model

3.2.1. Experimental Case in Regular Waves

An experimental case tested in regular waves is employed for numerical model validation first. The testing conditions include a regular wave height of H_0 = 0.05 m, a regular wave period of T_0 = 1.5 s, and a vessel starboard that is perpendicular to the incident wave direction. The time histories of two typical motions of the vessel model are compared in Figure 5 between the experimental and numerical results. For the heaving amplitude in Figure 5a, the positive peaks in the numerical prediction are slightly larger than those in the experimental test, while the negative peaks are well-correlated. For the swaying motion in Figure 5b, the numerical amplitude also agrees well with experimental results. In addition, the numerical curve shape is more uniform, and the experimental negative peaks shift to the upstream of the time axis.

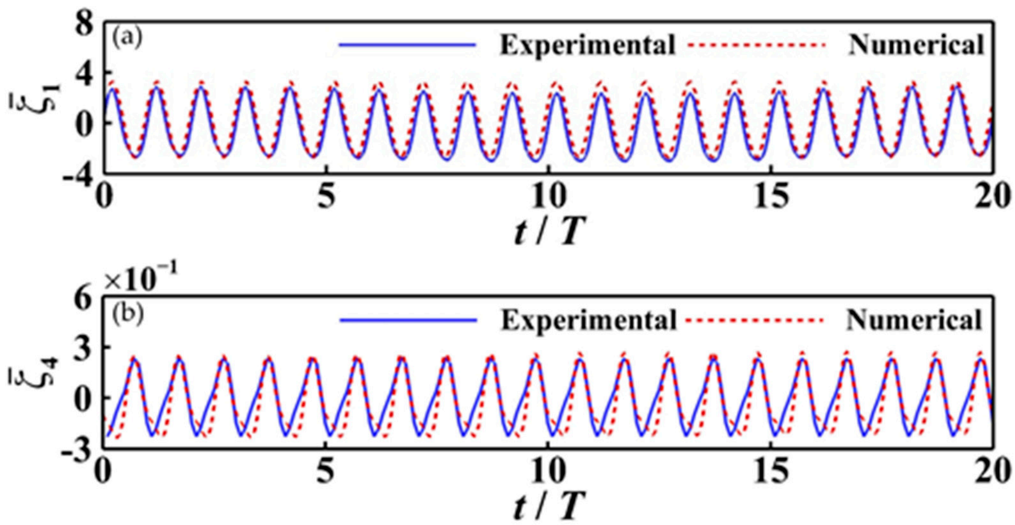

Figure 5. Time history comparisons between numerical and experimental results on two typical motions. (**a**) Heave. (**b**) Roll.

The comparison of nondimensional tensions in mooring lines between numerical and experimental results is shown in Figure 6. In most lines, the numerical model underestimated the tensions because more uncertainty factors influence the experimental testing process and results. The predicted results for four lines in the head waves have larger errors than the experimental data in the tension, while the differences between the four mooring lines on the other side are minor. Compared to the laboratory testing results, the numerical errors fall within a range from 5% to 12%.

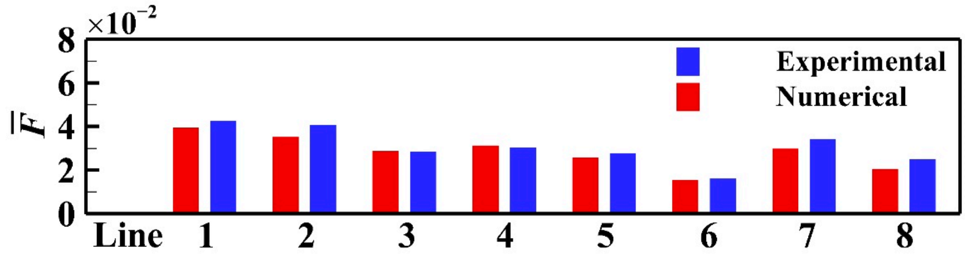

Figure 6. Comparison of average tensions in mooring lines between numerical and experimental results under the regular wave conditions.

3.2.2. Experimental Case in Irregular Waves

For the experimental case in irregular waves, the significant wave height and period are H_S = 0.041 m and T_S = 1.43 s with an incident direction perpendicular to the vessel hull. The comparison of peak amplitudes in the heaving and rolling motions between numerical and experimental results are shown in Figure 7. The numerical predictions overestimated the maximum amplitudes of the heaving and rolling motions because they were conducted in an idealized environment. Meanwhile, the experimental setup had several restrictions, such as the wave reflection by the end wall, bottom friction, and system errors from the measuring system for the model scale.

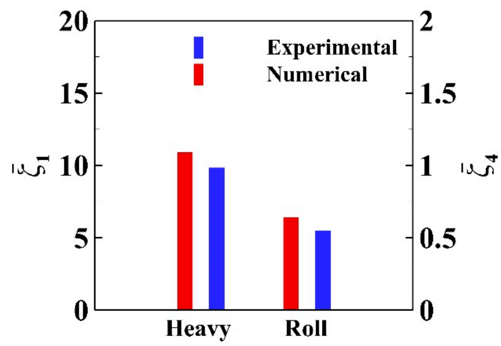

Figure 7. Comparison of peak amplitudes on two typical motions between numerical and experimental results.

The validation results of the numerical model on the tensions in mooring lines are shown in Figure 8. The numerical predictions on the average tensions in most mooring lines are overestimated, except for Line 1. In addition, the differences in the tensions of mooring lines in the head waves between numerical and experimental results are larger than those in the four lines on the other side. The average error of the numerical model for the irregular wave condition is approximately 10.5%, which is significantly larger than that in the regular wave condition because of the difficulties in force recording for the waves with smaller wave heights and periods. Regardless, the numerical model in this study shows reasonable accuracy in the prediction of critical performance indicators and will be employed in further investigations.

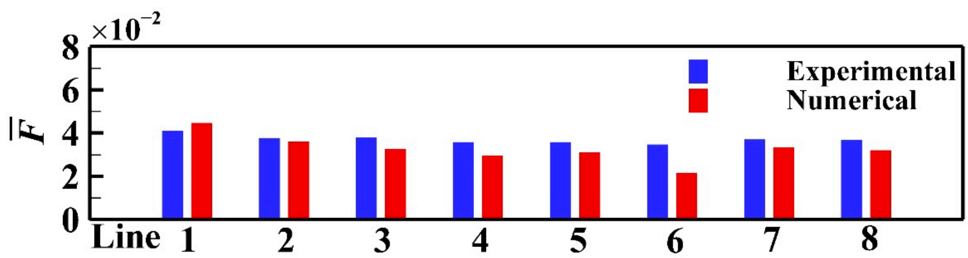

Figure 8. Comparison of average tensions in mooring lines between numerical and experimental results under the irregular wave condition.

4. Operating Performance in Actual Sea Conditions

4.1. Design of Testing Conditions

The numerical simulations for the vessel and submarine cable were all conducted at the prototype scale, which were set in Cartesian coordinates, as shown in Figure 9. The intersection angles of Lines 1 and 2 with the vessel hull are 22.5° and 112.5°, respectively. The other three series of mooring lines follow the same deployment format. The submarine cable is pulled from the center of the shipboard and the distance from the vessel to the anchor point on the coast is defined as L_c. The diameters and elasticity moduli of the mooring line and submarine cable are D_M = 0.05 m, D_C = 0.25 m, E_M = 6.9 × 10^3 MPa, and E_C = 4.5 × 10^3 MPa, respectively.

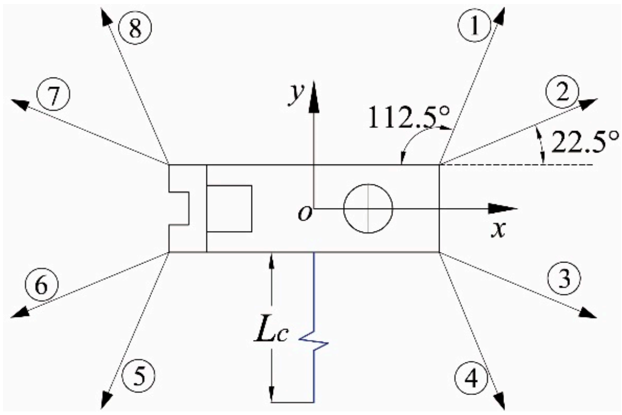

Figure 9. The vessel with mooring lines ①–⑧ and the submarine cable in Cartesian coordinates.

The sea around the Zhoushan Islands is considered the operating area, which has a great demand for submarine cable connections between islands. The water depth is between 5.0 m and 13.0 m with a maximum value of 50.0 m. The current velocity is approximately 4.0 knots, and the wind speed is around 6.0 m. The oceanic environmental factors are designed and listed in Table 2 as typically representative of sea conditions. As the vessel is close to the costal line during the cable-deploying operation, only the longshore current is considered with an incident direction of 180°. There are 16 testing cases in total required for further investigation.

Table 2. Designed oceanic environmental factors.

Factors	Designed Parameters	
Incident waves	H_S = 1.0 m T_S = 5.0 s	Direction [1] w: −45°, −90°, −135°
Current	Velocity (m/s): 1.5, 2.0, 2.5	Direction [1]: 180°
Wind	Wind speed: 6.0 m/s	Direction [1] f: 0, −45°, −90°, −135°, −180°
Length of submarine cable L_C	500.0 m, 520.0 m, 540.0 m, 560.0 m	

[1] Definition of direction: positive for counterclockwise rotation and negative for clockwise rotation from the positive x-axis in Figure 9.

4.2. Effects of the Submarine Cable Length

Based on typical operating conditions, four typical lengths of submarine cable are chosen in this section, as listed in Table 2. The incident current velocity is 2.0 m, and the incident wave and wind directions are w = −90° and f = −45°, respectively.

The effects of the submarine cable length on the peak amplitudes of the vessel motions are shown in Figure 10. As the cable length increases, the nondimensional values of the sway, surge, and roll increase. The peak values of $\overline{\zeta}_2$ and $\overline{\zeta}_3$ both exceed 20.0, while the peak value of $\overline{\zeta}_4$ is close to 1.0. The amplitude of yaw first increases and then converges as the value of L_C increases, while the heaving and pitching motions show little difference.

The decrease in buoyancy caused by the reduction in cable length results in an increase in the mooring function of the cable, and subsequently, the motions of the vessel all decrease. For a longer cable, the stability of the vessel is mainly provided by the mooring lines. The scattered dots on the right side represent motions without a submarine cable, which are larger than those with a cable.

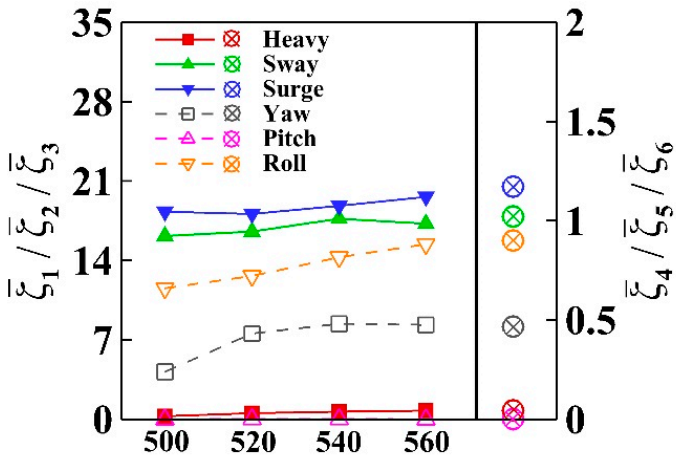

Figure 10. Effects of the submarine cable length on the vessel motions.

The effects of the submarine cable length on the tensions in the mooring lines and the cable are illustrated in Figure 11. As shown in Figure 11a, the tensions in Line 7 and 8 are larger than for the other cables because they are deployed in head waves to stabilize the vessel. As the cable length decreases, the peak values of the mooring line tensions all increase. For L_C = 500.0 m, the peak nondimensional tension in Line 8 of 0.071 is the maximum for all eight lines, which is much less than the safe threshold value of 1.0. For the average values of the tension in the mooring lines in Figure 11b, the distribution patterns are similar to those of the peak values. Furthermore, from Figures 10 and 11, the increase in the cable length results in a buoyancy increase due to the floaters and a decrease in the tension of the cable. Although the decrease in the cable length causes an increase in the vessel stability, the tension in the cable also significantly increases, and the insecurity of the cable also increases. Therefore, during deployment a floating length of the cable is maintained to keep it safe.

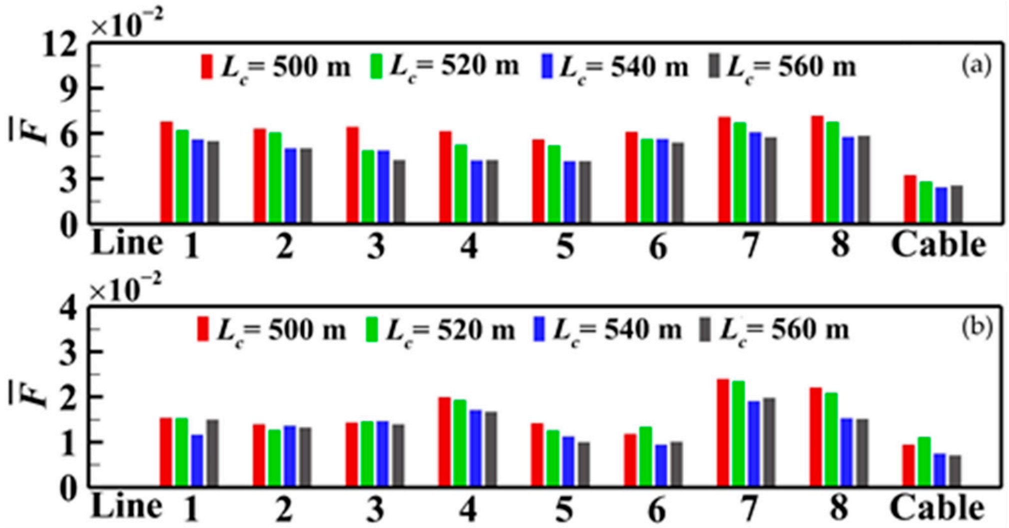

Figure 11. Effects of the submarine cable length on the tensions in the mooring lines and the cable. (**a**) Peak values. (**b**) Average values.

4.3. Effects of the Incident Current Velocity

The longshore current is the most critical type of current during cable landing from the vessel to the shore. Three values of the current velocity are employed in this study: 1.5 m/s, 2.0 m/s, and 2.5 m/s. Other typical operating conditions include: L_C = 500.0 m, $w = -90°$, and $f = -45°$.

The effects of the current velocity on the vessel stability are shown in Figure 12. The surging and swaying motions increase with the maximum nondimensional values of 20.6 and 17.7 as the current velocity increases due to the current acting on the vessel and the submarine cable. The dynamic positioning system is activated under large velocity conditions to stabilize the vessel. In addition, the rolling and yawing motions are restricted due to the tensioning cable as the current velocity increases. On the other hand, variations in the current velocity have little effect on the heaving and pitching motions, the values of which are minor.

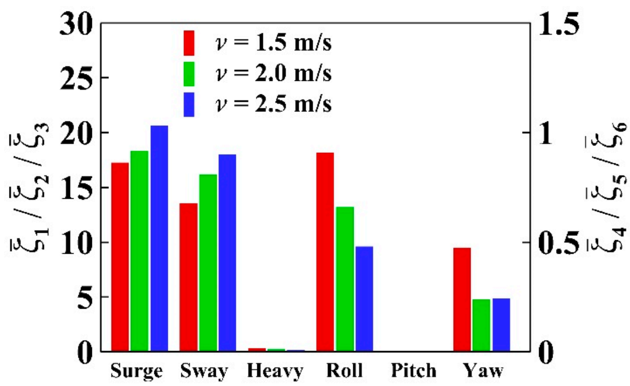

Figure 12. Effects of the incident current velocity on the vessel motions.

The effects of the incident current velocity on the tensions in the mooring lines and the cable are illustrated in Figure 13. The peak and average values of the tensions in the mooring lines and the cable all increase with an increase in the current velocity. Moreover, the mooring lines in head waves have larger tensions, which are focused on during the operation. During cable landing, the cable has a horizontal shift due to the current acting forces, and a significant increase in the cable tension can be observed. During cable deployment, if the current velocity is too great, the anchor boat is advised to push the floating cable to suitable positions to prevent over bending and over loading.

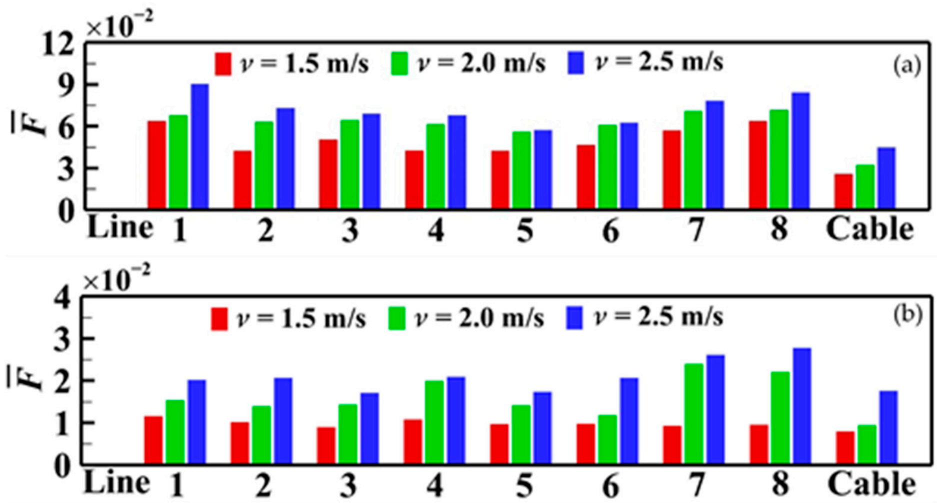

Figure 13. Effects of the incident current velocity on the tension in the mooring lines and the cable. (**a**) Peak values. (**b**) Average values.

4.4. Effects of the Incident Wave Direction

As the directions of the vessel and the current are determined by the cable-deploying operations, the incident wave direction is varied to identify the most negative method of offshore operation. Three incident wave directions were employed in this study: −45°, −90°, and −135°. Other typical operating conditions include L_C = 500.0 m, a current velocity of 2.0 m/s, and f = −45°.

The effects of the incident wave direction on the vessel stability are shown in Figure 14. As the wave direction changes from −45° to −135°, the vessel bow is under the attack of the waves, resulting in a significant increase in surging motion with a maximum amplitude of 26.1. As w = −90°, the incident wave direction is perpendicular to the vessel hull, resulting in the maximum amplitudes of the swaying and rolling motions. In addition, for w = −45° and −135°, the yawing amplitude is increased due to the oblique wave-acting forces.

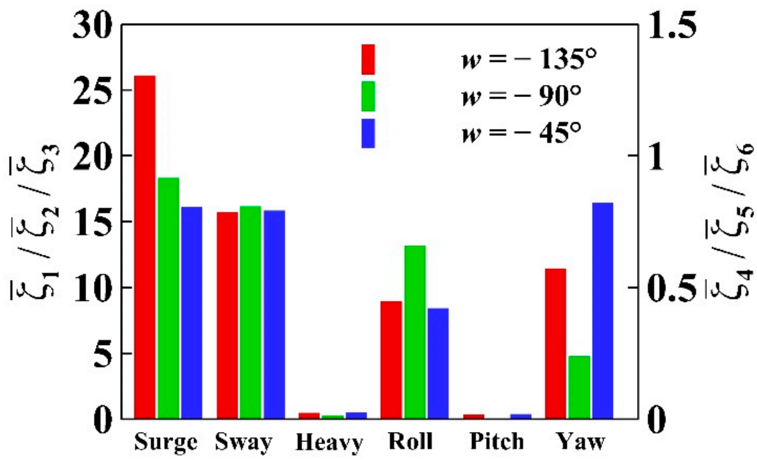

Figure 14. Effects of the incident wave direction on the vessel motions.

The effects of the incident wave direction on the tensions in the mooring lines and the cable are illustrated in Figure 15. For w = −45°, as shown in Figure 15a, the vessel stern is under the attack of the incident waves, resulting in larger tensions in Lines 5–8 with a maximum nondimensional tension in Line 7 of 0.075. On the other hand, for w = −135°, the vessel bow is under the wave attack, with the maximum tension on Line 4 of 0.074. If possible, a dynamic positioning system is recommended to provide additional power to the bow and stern of the vessel under these two directions of incident waves.

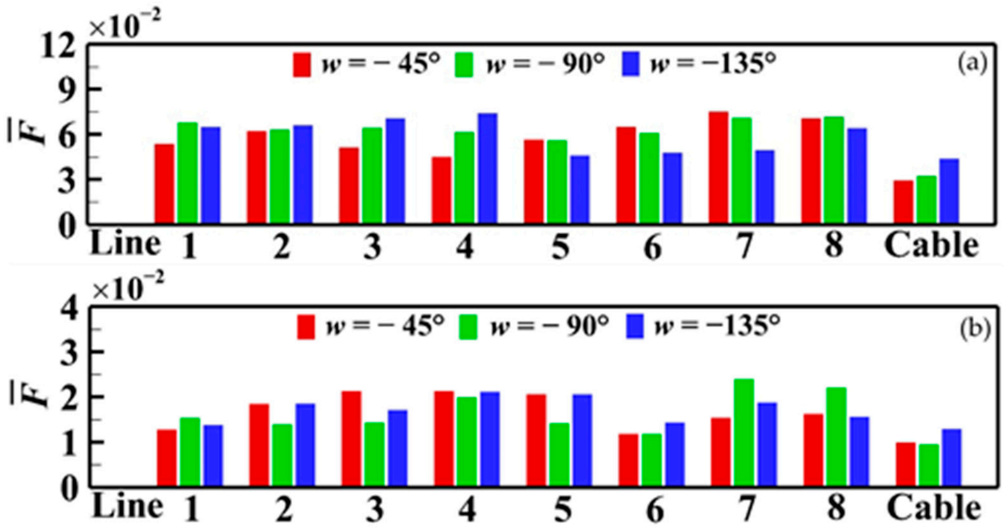

Figure 15. Effects of the incident wave direction on the tensions in the mooring lines and the cable. (**a**) Peak values. (**b**) Average values.

For the average tensions in Figure 15b, the values for different mooring lines have minor differences, and the distribution pattern is similar to that of the peak values. As $w = -135°$, the incident waves and current have joint acting forces on the submarine cable, and the tension in the cable is the largest with a value of 0.046. Therefore, under this circumstance, the anchor boat is used to push the floating cable to reduce the tension, which may lead to damage.

4.5. Effects of the Incident Wind Direction

During the cable deployment, the incident wind is another random environmental factor. As the wave direction of $w = -135°$ is identified as the most negative one, it is employed in the tests in this section. Five incident wind directions are employed in this study: 0, $-45°$, $-90°$, $-135°$, and $-180°$. Other typical operating conditions include L_C = 500.0 m and the current and wind velocities of 2.0 m/s and 6.0 m/s, respectively.

The effects of the incident wind direction on the vessel motions are shown in Figure 16. As the wind direction changes from 0 to $-180°$, the surging motion of the vessel is significantly enhanced, and a maximum nondimensional value of 22.5 is obtained. As $f = -90°$, the vessel is affected by the wind perpendicular to the hull, resulting in maximum swaying and rolling amplitudes with the same distribution pattern. Under these circumstances, the dynamic positioning system or the barge shall be employed to push the vessel and maintain the stability of the cable laying vessel. As the wind direction is parallel to the hull, the yaw motion is minor, while the maximum nondimensional yaw amplitude is obtained as 0.88. In addition, the heaving and pitching amplitudes are both minor.

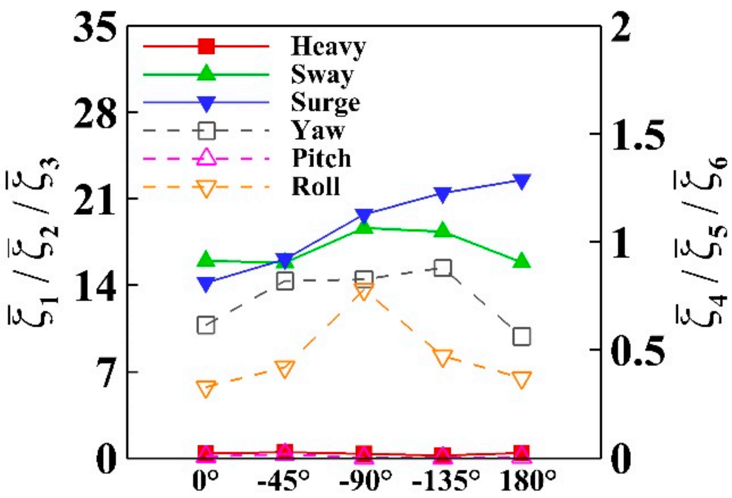

Figure 16. Effects of the incident wind direction on the vessel motions.

The effects of the incident wind direction on the tensions in the mooring lines and the cable are illustrated in Figure 17. For the peak values in Figure 17a, as the vessel bow is exposed to the incident wind ($f = -180°$), the peak tensions in Lines 1–4 are on average 23.4% larger than those in Lines 5–8; as the stern faces towards the wind ($f = 0$), the peak tensions in Lines 5–8 are on average 28.6% larger than those in Lines 1–4. The average tension values in Figure 17b have the same varying trend and distribution pattern as the peak values. For the submarine cable, as $f = -135°$ and $f = 180°$, the joint acting forces by the wave, wind, and current can be observed through the larger amplitude of the tension. Therefore, as the directions of the environmental forces tend to be the same, the tension in the cable is enhanced and the safety coefficient decreases, which should be avoided during cable landing operations.

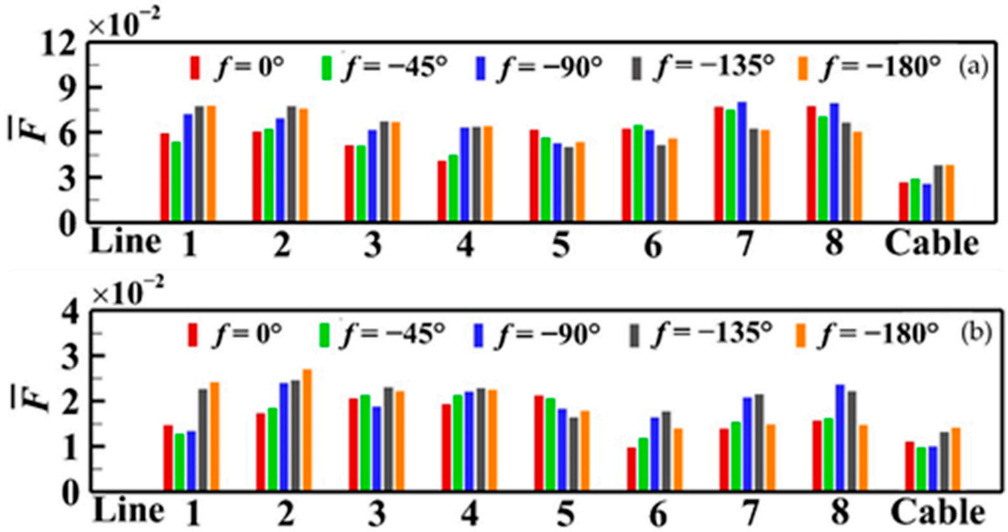

Figure 17. Effects of the incident wind direction on the tensions in the mooring lines and the cable. (**a**) Peak values. (**b**) Average values.

5. Conclusions

A numerical model was established based on Ansys-AQWA to simulate the dynamic interactions between a cable-laying vessel and a submarine cable during the cable landing process. The model was carefully validated by experimental data gleaned from a moored vessel model tested in a wave tank.

As the length decreases, the floating submarine cable with the floaters acts more like a mooring line for the vessel and enhances its stability with a significant increase in its tension. A stronger current increases the perpendicular forces acting on the cable, and the surging and swaying motions of the vessel are enhanced with increased tensions in both the mooring lines and the submarine cable. As the incident wave direction is $-135°$, the vessel is exposed to more positive impacts from the waves and the surging and rolling amplitudes are greater than those of the other DOFs. The joint effects from the waves and current cause the largest tension in the cable.

If the incident wind direction is parallel to the vessel hull, the wind has a minor influence on yawing motion, while its amplitude is enhanced at a wind direction of $-135°$. In addition, the tension in the cable is greatest under this wind direction due to the joint effects of all environmental forces, which should be avoided during the cable-laying process; otherwise, more safety steps should be implemented during operations.

Author Contributions: Conceptualization, Z.L.; methodology, J.K.; software, J.K., G.C. and Z.Y.; validation, G.C. and X.Q.; formal analysis, G.C., Z.Y. and X.Q.; writing—original draft preparation, Q.Y.; writing—review and editing, J.K. and Z.L.; visualization, J.K. All authors have read and agreed to the published version of the manuscript.

Funding: This research was funded by the Critical Technology Research Project on the Cable Landing Floaters, grant number 20190141.

Institutional Review Board Statement: Not applicable.

Informed Consent Statement: Not applicable.

Data Availability Statement: Not applicable.

Conflicts of Interest: The authors declare no conflict of interest.

References

1. Zhang, R.; Shen, G.Q.P.; Ni, M.; Wong, J.K.W. An overview on the status quo of onshore and offshore wind power development and wind power enterprise localization in China. *Int. J. Green Energy* **2019**, *16*, 1646–1664. [CrossRef]
2. Randolph, M.F.; Gaudin, C.; Gourvenec, S.M.; White, D.J.; Boylan, N.; Cassidy, M.J. Recent advances in offshore geotechnics for deep water oil and gas developments. *Ocean. Eng.* **2011**, *38*, 818–834. [CrossRef]
3. Zeng, Q.; Wang, Y.; Su, D. Safety Control of a Multiple Return 500 kV Submarine Cable Landing Project. *Soil Eng. Found.* **2018**, *32*, 10–14.
4. Evans, G.; Page, M. The planning and surveying of submarine cable routes. In *Submarine Cables*; Brill Nijhoff: Singapore, 2014; pp. 91–122.
5. Zhang, Z.; Dong, Y.; Yuan, Z.; Liu, Z. Innovative floating support technologies for submarine cable landing. In *Emerging Developments in the Power and Energy Industry*; CRC Press: Boca Raton, FL, USA, 2019; pp. 78–86.
6. Hu, Y.; Hu, Z.; Liu, Y.; Liu, J. Analysis of the large LNG ships moored against a quay based on AQWA. *Ship Sci. Technol.* **2012**, *34*, 70–73+110. [CrossRef]
7. Shigunov, V.; el Moctar, O.; Schellin, T.E.; Kaufmann, J.; Stute, R. Assessing the Dynamic Stability of an Offshore Supply Vessel. *J. Offshore Mech. Arct. Eng.* **2012**, *134*, 29–37. [CrossRef]
8. Liu, X.; Li, J. The Analysis of Some Deep-Sea Functional Ship's Structural Strength Based on AQWA. *Shipbuild. Vocat. Educ.* **2015**, *3*, 14–18. [CrossRef]
9. Putra, G.L.; Wibowo, H.T.; Agusta, F. Stability analysis of semi-trimaran flat hull ship for a sea transportation model. *Commun. Sci. Technol.* **2017**, *2*, 42–46. [CrossRef]
10. Roy, S.; Ghosh, V.; Dey, S.; Vimmadi, S.; Banik, A.K. A coupled analysis of motion and structural responses for an offshore spar platform in irregular waves. *Ships Offshore Struct.* **2017**, *12*, S296–S304. [CrossRef]
11. Banik, A.K.; Roy, S.; Saha, K.; Dey, S. Effect of wave spreading including multi-directional wave interaction on the responses of a spar platform. *Mar. Syst. Ocean. Technol.* **2019**, *14*, 153–165. [CrossRef]
12. Wang, L.; Tang, Y.; Zhang, X.; Zhang, J. Studies on parametric roll motion of ship under wave group by numerical simulation. *Ocean. Eng.* **2018**, *163*, 391–399. [CrossRef]
13. Su, Y.; Wang, J.; Zhuang, J.; Shen, H.; Bi, X. Experiments and CFD of a variable-structure boat with retractable twin side-hulls: Seakeeping in waves. *Ocean. Eng.* **2021**, *235*, 109358. [CrossRef]
14. Liu, Y. Dynamic Analysis of Mooring Cables and Their Damping Effect on the Low-Frequency Motion of Floating Platforms. Ph.D. Thesis, Chalmers University of Technology, Gothenburg, Sweden, 1997.
15. Sarkar, A.; Taylor, R.E. Effects of mooring line drag damping on response statistics of vessels excited by first-and second-order wave forces. *Ocean. Eng.* **2000**, *27*, 667–686. [CrossRef]
16. Sarkar, A.; Taylor, R.E. Dynamics of mooring cables in random seas. *J. Fluids Struct.* **2002**, *16*, 193–212. [CrossRef]
17. Gao, F.; Li, Y.; Shen, W.J. Test study on mooring characteristic for multi-body floating system under the action of wind, wave and flow. *J. Waterw. Harb.* **2017**, *38*, 555–560.
18. Mengxi, N.; Xusheng, W.; Xiaoming, W.; Lin, Z. Time domain approach for computing the mooring force of a mooring system subject to wind, waves and currents. *J. Tsinghua Univ.* **2004**, *9*, 1214–1217. [CrossRef]
19. Zheng, W.; Li, J.; Liu, S.; Sun, Y. Research on tensions of bow stern mooring of single ship under the combination impact of external environmental load factors. *J. Waterw. Harb.* **2016**, *37*, 490–496.
20. Pham, N.D.K.; Nguyen, X.P. Application of CFD for calculation and simulation of anchor-cable tensions in mooring ship. *J. Mech. Eng. Res. Dev.* **2019**, *42*, 182–186. [CrossRef]
21. Nguyen, X.P.; Pham Nguyen, D.K. Experimental Research on the Impact of Anchor-Cable Tensions in Mooring Ship at Vung Tau Anchorage Area. *Int. J. Adv. Sci. Eng. Inf. Technol.* **2019**, *9*, 1892–1899. [CrossRef]
22. Mingyu, F.; Aihua, Z.; Jinlong, X.; Jianfang, J. Adaptive dynamic surface tracking control for dynamic positioning cable laying vessel. In Proceedings of the 2012 IEEE International Conference on Automation and Logistics, Zhengzhou, China, 15–17 August 2012; pp. 266–271.
23. Yang, N.; Jeng, D.; Zhou, X. Tension analysis of submarine cables during laying operations. *Open Civ. Eng. J.* **2013**, *7*, 282–291. [CrossRef]
24. Tommasini, R.B.; de Oliveira Carvalho, L.; Pavanello, R. A dynamic model to evaluate the influence of the laying or retrieval speed on the installation and recovery of subsea equipment. *Appl. Ocean Res.* **2018**, *77*, 34–44. [CrossRef]
25. Cavefors, J.; Oscarsson, A. *Vessel Motions and Mooring Line Tensions in Very Shallow Water*; Chalmers University of Technology: Gothenburg, Sweden, 2016.
26. Zhang, D.; Bai, Y.; Zhao, W.; Zhu, K. Dynamic analysis of submarine cable during the process of laying back to the seabed. *Ships Offshore Struct.* **2020**, *15*, 153–161. [CrossRef]
27. Wang, Y.; Bian, X.; Zhang, X.; Xie, W. A study on the influence of cable tension on the movement of cable laying ship. In Proceedings of the OCEANS 2010 IEEE, Seattle, WA, USA, 20–23 September 2010.
28. Srikanth, N.; Rao, S.S. Subsea cable health monitoring system. In Proceedings of the 2017 Asian Conference on Energy, Power and Transportation Electrification (ACEPT) IEEE, Singapore, 24–26 October 2017; pp. 1–9.
29. Nexans. Available online: https://www.nexans.com/en/ (accessed on 23 May 2022).
30. Drissi-Habti, M.; Abhijit, N.; Sriharsha, M.; Carvelli, V.; Bonamy, P.-J. Concept of Placement of Fiber-Optic Sensor in Smart Energy Transport Cable under Tensile Loading. *Sensors* **2022**, *22*, 2444. [CrossRef] [PubMed]

31. Newman, J.N. *The Theory of Ship Motions: Advances in Applied Mechanics*; Elsevier: Amsterdam, The Netherlands, 1979; Volume 18, pp. 221–283.
32. Ghafari, H.; Dardel, M. Parametric study of catenary mooring system on the dynamic response of the semi-submersible platform. *Ocean. Eng.* **2018**, *153*, 319–332. [CrossRef]
33. Lu, Z.; Cao, C.; Ge, Y.; He, J.; Yu, Z.; Chen, J.; Zheng, X. Research on Improving the Working Efficiency of Hydraulic Jet Submarine Cable Laying Machine. *J. Mar. Sci. Eng.* **2021**, *9*, 745. [CrossRef]
34. Nexans. Lavrio Syros Interconnector Project. Available online: https://www.nexans.com/business/High-Voltage---Projects/Power-Networks-Subsea-Power-Cables/Lavrio---Syros.html,2017 (accessed on 15 October 2021).
35. Wang, W.; Wu, M.; Palm, J.; Eskilsson, C. Estimation of numerical uncertainty in computational fluid dynamics simulations of a passively controlled wave energy converter. *J. Eng. Marit. Environ.* **2018**, *232*, 71–84. [CrossRef]